Onset of convection with temperature- and depth-dependent viscosity

Jun Korenaga

Department of Earth and Planetary Science, University of California, Berkeley, CA, USA

Thomas H. Jordan

Department of Earth Sciences, University of Southern California, Los Angeles, CA, USA

[1]   We derive a scaling law for the onset of convection in an incompressible fluid cooled from above with temperature- and depth-dependent viscosity, on the basis of 2-D numerical simulation. Rayleigh numbers up to 10^7 are considered. The activation energy is varied from 0 to 200 kJ mol^{-1}, and a variation of up to 10^3 is considered in depth-dependent reference viscosity. Our scaling law is shown to be able to handle a variety of buoyancy distributions, including highly non-Gaussian and multimodal distributions, with a tightly constrained critical Rayleigh number.   *INDEX TERMS:* 3035 Marine Geology and Geophysics: Midocean ridge processes; 8121 Tectonophysics: Dynamics, convection currents and mantle plumes; 8162 Tectonophysics: Evolution of the Earth: Rheology—mantle. **Citation:** Korenaga, J., and T. H. Jordan, Onset of convection with temperature- and depth-dependent viscosity, *Geophys. Res. Lett.*, *29*(19), 1923, doi:10.1029/2002GL015672, 2002.

1.   Introduction

[2]   The onset of convection in a fluid cooled from above is a simple fluid dynamical problem, with profound applications for the dynamics of the Earth's mantle. Because of the strong temperature dependency of mantle rheology, most of temperature variations in mantle convection are confined in a cold and stiff boundary layer (lithosphere), the dynamics of which dominates the global energetics of mantle convection [e.g., *Conrad and Hager*, 1999]. The thickness of the boundary layer is one of essential controlling parameters in such energetics. Thicker lithosphere requires greater energy to be dissipated for its deformation at subduction zones. The growth of the boundary layer is limited by its intrinsic convective instability, which is characterized by the onset of convection [e.g., *Parsons and McKenzie*, 1978; *Yuen and Fleitout*, 1984; *Buck and Parmentier*, 1986; *Davaille and Jaupart*, 1994].

[3]   A scaling law for the onset of convection has already been established for the case of temperature-dependent viscosity [*Korenaga and Jordan*, 2002]. The purpose of this paper is to extend it to a more general case, i.e., temperature- and depth-dependent viscosity. This generalization is important because mantle melting beneath mid-ocean ridges is expected to introduce intrinsic rheological layering in the shallow upper mantle [e.g., *Karato*, 1986; *Hirth and Kohlstedt*, 1996]. Residual mantle after melting,

which normally occupies the upper 60–80 km of the oceanic mantle, could be by two orders of magnitude more viscous than unmelted mantle.

[4]   Our approach is based on two-dimensional numerical simulation, in a manner similar to *Korenaga and Jordan* [2002]. Depth-dependent viscosity introduces one significant challenge for scaling analysis. Buoyancy density distribution becomes highly non-Gaussian and can even become multimodal. We will demonstrate that the concept of the differential Rayleigh number is still valid for non-Gaussian buoyancy distribution, and also that multimodal distribution can be treated successfully by considering the coupling of sub-distributions.

2.   Numerical Modeling

[5]   The numerical formulation is basically the same as that described by *Korenaga and Jordan* [2002], except for the addition of depth-dependent viscosity (Figure 1). Only key elements are summarized here. The governing equations for thermal convection of an incompressible fluid are integrated by the finite element method. Length and time are normalized by a system depth, D, and a diffusion time, D^2/κ, respectively, where κ is thermal diffusivity. Temperature is normalized by ΔT, which is the difference between the initial fluid temperature (T_0) and the imposed surface temperature (T_s). Viscosity is normalized by μ_0, which is reference viscosity measured at the model base with the initial temperature. The superscript * denotes normalized variables. The aspect ratio of the model domain is unity, with rigid horizontal and reflecting vertical boundaries. The top and bottom temperature are fixed at 0 and 1, respectively. The initial internal temperature is set to unity plus random perturbations with the maximum amplitude of 10^{-5}. The convection system has one non-dimensional parameter called the Rayleigh number, which is defined as

$$Ra = \frac{\alpha \rho_0 g \Delta T D^3}{\kappa \mu_0} \quad (1)$$

where α is the coefficient of thermal expansion, g is gravitational acceleration, and ρ_0 is reference density at T_0. The following viscosity law is employed:

$$\mu(T^*, z^*) = \mu_r(z^*)\exp\left(\frac{E^*}{T^* + T_{\text{off}}^*} - \frac{E^*}{1 + T_{\text{off}}^*}\right), \quad (2)$$

where $E^* = E/(R\Delta T)$ and $T_{\text{off}}^* = 273/\Delta T$. E is activation energy, and R is the universal gas constant. ΔT is set to
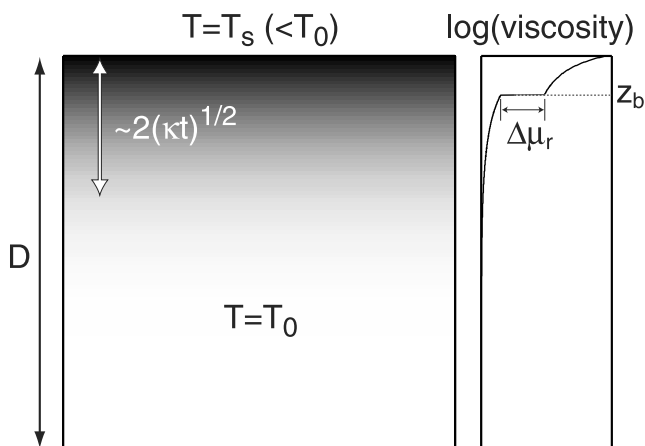
Figure 1. Model geometry and length scales of transient cooling. Gray scale indicates temperature variation. Onset of convection is significantly influenced by temperature- and depth-dependent viscosity.

1300. The z axis is downward. For the depth-dependent part, we use a simple two-layer model as

$$\mu_r(z*) = \begin{cases} \Delta\mu_r & 0 \le z* \le z_b^* \\ 1 & z_b^* < z* \le 1 \end{cases} \quad (3)$$

where $\Delta\mu_r$ is greater than unity. To ensure numerical stability, the largest normalized viscosity is limited to 10^5.

[6] The range of activation energy used is 0–30 kJ mol^{-1} for $Ra = 10^5$, 0–120 kJ mol^{-1} for $Ra = 10^6$, and 0–200 kJ mol^{-1} for $Ra = 10^7$. An increment in activation energy is 10 for $Ra = 10^5$ and 10^6 and 20 for $Ra = 10^7$, which amounts to 28 different cases. Combined with all possible combinations of $z_b^* = 0.1$, 0.25, and 0.5 and $\Delta\mu_r = 10$, 10^2, and 10^3, we conducted total 252 runs of the instantaneous cooling model. The onset time of convection, t_c^*, is defined as when a horizontally averaged temperature profile deviates from a purely conductive profile by greater than 0.01 at any depth level. Because of the rapid growth of convective instability, our measurement is not very sensitive to this particular value of the threshold. In the following, we focus on the runs in which convection took place before a conductive cooling front reaches the model bottom (i.e., $t_c^* < \sim 0.06$), so that the development of convective instability is least influenced by finite-domain effects. The number of such runs is 189.

[7] Our measurements of onset time are summarized in Figure 2. Onset times, t_c^*, are normalized by the local timescale for boundary-layer instabilities, $t_r^* = Ra^{-2/3}$, and they are plotted as a function of E. The effect of depth-dependent viscosity can be readily seen in the systematics of onset time. Our task is to develop a general scaling law to explain the observed systematics.

3. Scaling Analysis

[8] Our scaling analysis is based on the concept of the differential Rayleigh number, which has been introduced by *Korenaga and Jordan* [2002]. Because of intrinsic depth-dependent viscosity, however, a similarity variable,
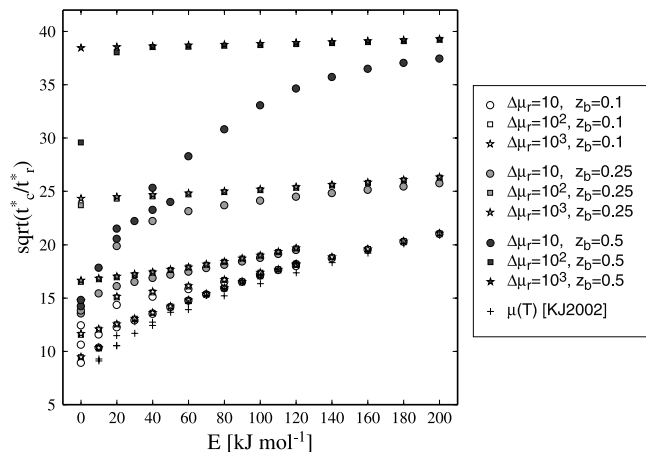

Figure 2. Summary of onset time measurements in terms of the activation energy E and the square root of onset time (t_c^*) scaled by local boundary-layer time scale ($t_r^* = Ra^{-2/3}$). Data for purely temperature-dependent cases are from *Korenaga and Jordan* [2002].

$\eta = z.*/(2\sqrt{t*})$, cannot be used, and the present analysis is formulated with two independent variables, i.e., $z*$ and $t*$. Following *Howard* [1966], we assume that convection takes place when the local Rayleigh number reaches a critical value as,

$$Ra_\delta(t_c^*) = R_c. \quad (4)$$

To calculate Ra_δ, we first define the distribution of available buoyancy density as

$$\beta(z*, t*) = \frac{1}{\mu*}\frac{dT*}{dz*}. \quad (5)$$

Some examples of β are shown in Figure 3. They are all highly non-Gaussian, unlike the cases of temperature-
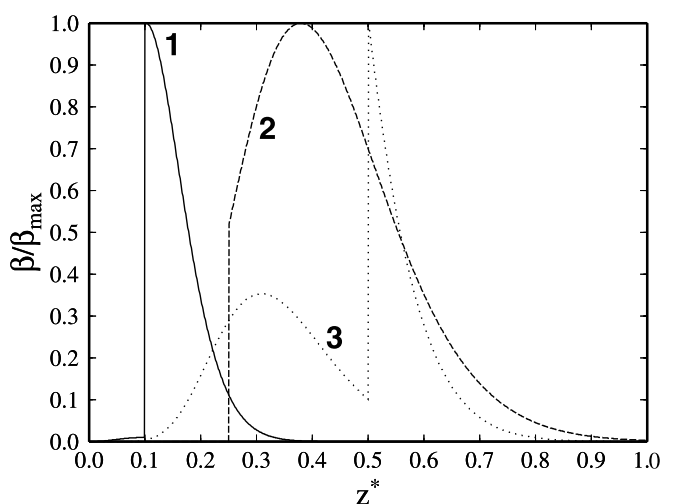

Figure 3. Examples of buoyancy density distribution $\beta(z*, t_c^*)$. Case 1 (solid): $Ra = 10^7$, $E = 20$, $z_b^* = 0.1$, $\Delta\mu_r = 10^2$, and $t_c^* = 4.88 \times 10^{-3}$. Case 2 (dashed): $Ra = 10^6$, $E = 70$, $z_b^* = 0.25$, $\Delta\mu_r = 10^3$, and $t_c^* = 3.29 \times 10^{-2}$. Case 3 (dotted): $Ra = 10^7$, $E = 80$, $z_b^* = 0.5$, $\Delta\mu_r = 10$, and $t_c^* = 2.05 \times 10^{-2}$.

dependent viscosity studied by *Korenaga and Jordan* [2002]. The origin of available buoyancy may be calculated as

$$z_o^* = z_m^* - \beta^{-1}(z_m^*, t^*) \int_0^{z_m^*} \beta(z^*, t^*) dz^* \qquad (6)$$

where $\beta(z_m^*, t^*) = \max \beta(z^*, t^*)$. The differential Rayleigh number is then defined as

$$dRa = \frac{4\alpha\rho_0 g \Delta T (z^* - z_o^*)^3 D^3}{\kappa\mu} \frac{dT^*}{dz^*} dz^*. \qquad (7)$$

The local Rayleigh number is obtained by integrating this differential Rayleigh number as

$$Ra_\delta(t^*) = \int_0^1 dRa \qquad (8)$$

$$= Ra \cdot F(t^*) \qquad (9)$$

where $F(t^*)$ is a functional that depends on buoyancy density as

$$F(t^*) = \int_0^1 4(z^* - z_o^*)^3 \beta(z^*, t^*) dz^*. \qquad (10)$$

It can be shown that the functional F is approximately (total available buoyancy) × (width of buoyancy distribution)^3. For a time-independent linear temperature profile (i.e., $dT^*/dz^* = 1$) and uniform viscosity, $F = 1$. Our R_c is related to the conventional critical Rayleigh number as $Ra_c = (\pi^2/2^5)R_c$ [*Korenaga and Jordan*, 2002]. From equations (4) and (9), therefore, we have

$$Ra_c = \frac{\pi^2}{2^5} Ra \cdot F(t_c^*). \qquad (11)$$

The success of the scaling analysis may be measured by the variance of Ra_c calculated from our modeling results using equation (11).

[9] Estimated values for Ra_c, based on equations (6), (10), and (11), are shown in Figure 4a. Most of estimates fall in the range of 1500–3000, which translates into about ±20% error in the onset time of convection. Some systematic trends can be seen, which are probably because we vary the activation energy systematically, with the same random ensemble for the initial temperature field. Several significant outliers are also observed, which correspond to the cases with the bimodal distribution of buoyancy density. These outliers clearly indicate that a multimodal distribution must be treated with care. We may dissect a multimodal distribution into non-overlapping N sub-distributions, each with a single maximum, and calculate the functional F as

$$F(t^*) = \sum_{i=1}^{N} \int_{z_{si}^*}^{z_{ei}^*} 4(z^* - z_{oi}^*)^3 \beta(z^*, t^*) dz^*, \qquad (12)$$

where z_{si}^* and z_{ei}^* define the range of the i-th sub-distribution, and z_{oi}^* denotes its origin calculated in a
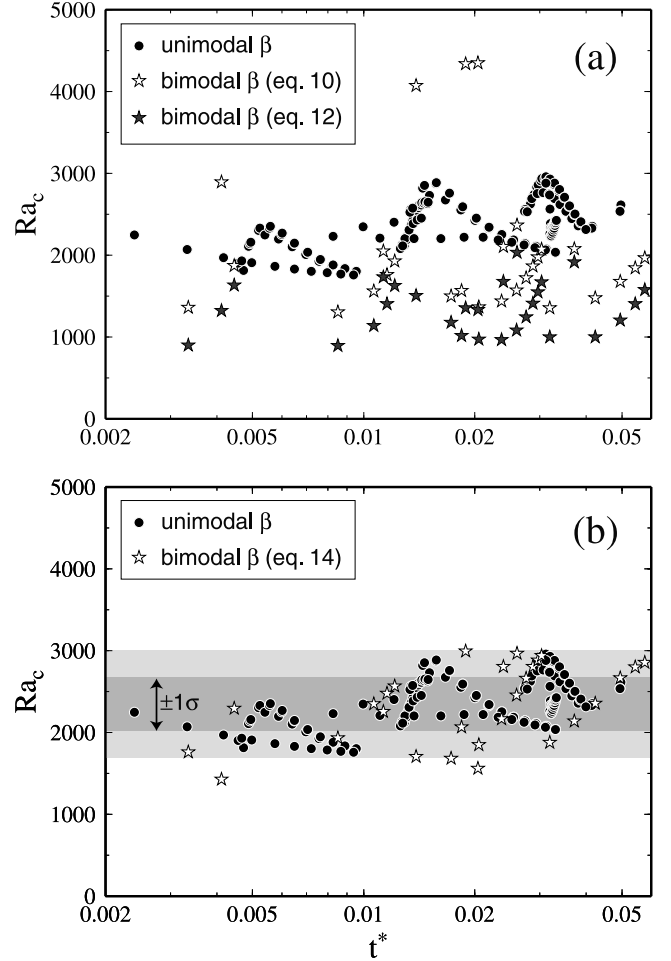

Figure 4. Estimated Ra_c as a function of onset time. (*a*) Ra_c for unimodal buoyancy distributions (solid circle) are confined in the rage of 1500–3000. Outliers correspond largely to bimodal distributions of buoyancy density. Open and solid stars denote Ra_c calculated with equations (10) and (12), respectively. (*b*) Ra_c becomes less scattered with the consideration of buoyancy coupling [equation (14) with $p = 1.5$]. Gray shadings show one and two standard deviations.

similar manner to equation (6). This formula, however, underestimates Ra_c, as shown in Figure 4a.

[10] This difficulty in defining a widely applicable functional F is rooted in the cubic dependence of the Rayleigh number on the length scale. Simple summation of F values corresponding to sub-distributions cannot represent the system's true convective instability. How, then, should we proceed?

[11] One may realize that the above subdivision is a rather arbitrary procedure. Consider, for example, a bimodal distribution. If two maxima of the distribution are located closely, with an insignificant minimum between them, the distribution may reasonably be approximated as unimodal. The functional F should not depend on whether this distribution is treated as unimodal or bimodal. Equations (10) and (12), however, give considerably different values. On the other hand, if two maxima are located far apart with a wide zero-buoyancy interval between them, we do not

expect that these two sub-distributions interact to produce system-wide convective instability. The concept of sub-distributions thus cannot be dropped. Adding up the convective instability of sub-distributions must be somehow capable of bridging smoothly the above two extreme cases.

[12] The simplest remedy appears to consider some kind of 'coupling' among sub-distributions. It is clear that such coupling should be inversely proportional to the separation between sub-distributions. An algebraic argument can also show that the coupling may be implemented in terms of a difference introduced by subdivision such as:

$$\Delta_i(z, t) \equiv (z - z_{o1})^3 - (z - z_{oi})^3$$
$$= 3(z_{oi} - z_{o1})z^2 - 3(z_{oi}^2 - z_{o1}^2)z + (z_{oi}^3 - z_{o1}^3), \quad (13)$$

where z_{oi} is a function of time. We thus define the functional F for a multimodal distribution as

$$F(t^*) = \sum_{i=1}^{N} \int_{z_{si}^*}^{z_{ei}^*} 4(z^* - z_{oi}^*)^3 \beta(z^*, t^*) dz^*$$
$$+ \sum_{i=2}^{N} (2\sigma_1 z_{si}^* - z_{s1}^*)^p \int_{z_{si}^*}^{z_{ei}^*} \Delta_i(z^*, t^*) \beta(z^*, t^*) dz^*, \quad (14)$$

where σ_1 is one standard deviation of the first sub-distribution, and p is an empirical exponent. We found that, with $p = 1.5$, all of our onset-time measurements may be explained by $Ra = 2350 \pm 330$ (Figure 4b).

[13] Considering various types of buoyancy distributions appeared in our modeling (e.g., Figure 3), the unifying scaling law for the onset of convection [equations (11) and (14)] can be considered to be quite successful. The wide range of temperature- and depth-dependent viscosity employed in this study ensures that our scaling law can safely be applied to the convective instability of thermal boundary layers in the Earth's mantle.

References

Buck, W. R., and E. M. Parmentier, Convection beneath young oceanic lithosphere: Implications for thermal structure and gravity, *J. Geophys. Res.*, *91*, 1961–1974, 1986.

Conrad, C. P., and B. H. Hager, The thermal evolution of an earth with strong subduction zones, *Geophys. Res. Lett.*, *26*, 3041–3044, 1999.

Davaille, A., and C. Jaupart, Onset of thermal convection in fluids with temperature-dependent viscosity: Application to the oceanic mantle, *J. Geophys. Res.*, *99*, 19,853–19,866, 1994.

Hirth, G., and D. L. Kohlstedt, Water in the oceanic mantle: Implications for rheology, melt extraction, and the evolution of the lithosphere, *Earth Planet. Sci. Lett.*, *144*, 93–108, 1996.

Howard, L. N., Convection at high Rayleigh number, in *Proceedings of the Eleventh International Congress of Applied Mechanics*, edited by H. Gortler. pp. 1109–1115, Springer-Verlag, New York, 1966.

Karato, S., Does partial melting reduce the strength of the upper mantle?, *Nature*, *319*, 309–310, 1986.

Korenaga, J., and T. H. Jordan, Physics of multi-scale convection in the Earth's mantle, 1, scaling laws, stability analysis, and 2-D numerical results, in revision, *J. Geophys. Res.*, 2002.

Parsons, B., and D. McKenzie, Mantle convection and the thermal structure of the plates, *J. Geophys. Res.*, *83*, 4485–4496, 1978.

Yuen, D. A., and L. Fleitout, Stability of the oceanic lithosphere with variable viscosity: an initial-value approach, *Phys. Earth Planet. Int.*, *34*, 173–185, 1984.

J. Korenaga, Department of Earth and Planetary Science, University of California, 377 McCone Hall, Berkeley, CA 94720-4767, USA. (korenaga@seismo.berkeley.edu)

T. H. Jordan, Department of Earth Sciences, University of Southern California, SCI 103, Los Angeles, CA 90089-0740, USA. (tjordan@usc.edu)